Propagating interfaces in mixtures of active and passive Brownian particles

2016 New J. Phys. 18 123030

(http://iopscience.iop.org/1367-2630/18/12/123030)

New Journal of Physics
The open access journal at the forefront of physics

Deutsche Physikalische Gesellschaft DPG
IOP Institute of Physics

Published in partnership with: Deutsche Physikalische Gesellschaft and the Institute of Physics

OPEN ACCESS

RECEIVED
6 September 2016

REVISED
21 November 2016

ACCEPTED FOR PUBLICATION
8 December 2016

PUBLISHED
23 December 2016

PAPER

Propagating interfaces in mixtures of active and passive Brownian particles

Adam Wysocki[1,2], **Roland G Winkler and Gerhard Gompper**

Theoretical Soft Matter and Biophysics, Institute of Complex Systems and Institute for Advanced Simulation, Forschungszentrum Jülich, D-52425 Jülich, Germany

[1] Present address: Theoretical Physics, Saarland University, Campus E2.6, D-66123 Saarbrücken, Germany.

[2] Author to whom any correspondence should be addressed.

E-mail: a.wysocki@lusi.uni-sb.de, r.winkler@fz-juelich.de and g.gompper@fz-juelich.de

Keywords: active matter, interface growth, phase separation

Supplementary material for this article is available online

Abstract

The emergent collective dynamics in phase-separated mixtures of isometric active and passive Brownian particles is studied numerically in two-dimensions. A novel steady-state of well-defined propagating interfaces is observed, where the interface between the dense and the dilute phase propagates and the bulk of both phases is (nearly) at rest. Two kind of interfaces, advancing and receding, are formed by spontaneous symmetry breaking, induced by an instability of a planar interface due to the formation of localized vortices. The propagation arises due to flux imbalance at the interface, resembling the growth behavior of rough surfaces far from equilibrium. Above a threshold, the interface velocity decreases linearly with increasing fraction of active particles.

1. Introduction

Ensembles of self-propelled particles are inherently out of equilibrium, which often gives rise to unexpected emergent behavior [1, 2]. From a physical perspective, the simplest systems are suspensions of self-propelled spheres. Strikingly, such systems exhibit clustering and motility-induced phase separation even in the absence of attraction and aligning interactions, as has been shown experimentally [3–6] and by simulations [7–10]. In theory and simulations, ensembles of self-propelled spheres are often modelled as active Brownian particles (ABPs) with short-range repulsive interactions [1, 2]. This is of course a simplification, since other interactions, like phoretic and hydrodynamic interactions, are neglected. However, this simplification helps to elucidate the pertinent effects which arise from the competition of self-propulsion, noise, and excluded volume interactions. The phase behavior and kinetics, like domain coarsening [8, 11] or interface fluctuations [12], of ABP fluids to some extent resembles the behavior of passive fluid with adhesion. Moreover, ABPs exhibit an intriguing collective dynamics with jets and swirls, which has been speculated to arise from interfacial sorting of ABPs with different orientations [9].

Even more interesting are mixtures of active and passive particles [13], which provide, for example, an novel route for switchable self-assembly [14], microrheological measurements [15], or even shed light on the active dynamical processes within the cell [16]. By now, only structural properties, like phase behaviour, in mixtures with different activities [13, 17–19], temperatures [20–22], or diameters [23] have been investigated. In particular, activity-induced phase separation has been observed in active–passive mixtures [13, 21, 24].

We focus here on the collective dynamics of mixtures of isometric active and passive Brownian particles over a wide composition range. Surprisingly, we find that these systems exhibit a novel and so far unexplored type of collective motion in the phase-separated state in the form of well-defined propagating interfaces, which can be either enriched or depleted of active particles, and are advancing toward or receding from the dense phase, respectively. The propagation arises due to flux imbalance of active and passive particles in the dilute phase. The fluctuation spectrum of these propagating interfaces shows the standard q^{-2} dependence on the wave number q

as equilibrium interfaces with tension for small q, but a faster decay for larger q. To account for the observed scaling of interface roughness and dynamics, we adapt an explanation based on well-studied models for the growth of rough surfaces under far-from-equilibrium conditions [25, 26].

2. Model

We simulate a mixture of N_A active and N_P passive Brownian disks (in total $N = N_A + N_P$ particles) in a 2D simulation box of size $L_x \times L_y$ with periodic boundary conditions. Their dynamics is overdamped, i.e., $\dot{\mathbf{r}}_i = V_0 \mathbf{e}_i + \mathbf{f}_i/\gamma_t + \boldsymbol{\xi}_i$, where V_0 is the propulsion velocity along the polar axis $\mathbf{e}_i$ ($V_0 = 0$ for passive particles), $\mathbf{f}_i = \sum_{i \neq j} \mathbf{f}_{ij}$ is the force due to steric interactions, and $\boldsymbol{\xi}_i$ is a random velocity. The particles interact via the soft repulsive force $\mathbf{f}_{ij} = k(a_i + a_j - |\mathbf{r}_{ij}|)\mathbf{r}_{ij}/|\mathbf{r}_{ij}|$, with $\mathbf{r}_{ij} = \mathbf{r}_i - \mathbf{r}_j$ if $a_i + a_j < |\mathbf{r}_{ij}|$ and $\mathbf{f}_{ij} = 0$ otherwise [7]. The discs are polydisperse in order to avoid crystallization and their radii a_i are uniformly distributed in the interval $[0.8a,\ 1.2a]$ [7]. The zero-mean Gaussian white-noise velocity $\boldsymbol{\xi}_i$ obeys $\langle \boldsymbol{\xi}_i(t)\boldsymbol{\xi}_i(t')\rangle = 2D_t\delta_{ij}\mathbf{1}\delta(t - t')$, where $D_t = k_B T/\gamma_t$ is the translational diffusion coefficient with thermal energy $k_B T$ and friction coefficient γ_t. The propulsion direction $\mathbf{e}_i$ undergoes a free rotational diffusion with a diffusion constant D_r, where $D_t/D_r = 4a^2/3$ holds for a no-slip sphere. The persistence of swimming is characterised by the Péclet number $\mathrm{Pe} = V_0/(2aD_r)$. The typical particle overlap due to activity, $\gamma_t V_0/(2ak)$, is fixed to 0.01 [11]. Unless otherwise noted, we consider systems with $\mathrm{Pe} = 100$ and a packing fraction $\phi = \sum_{i=1}^{N} \pi a_i^2/(L_x L_y) = 0.67$, below random closed packing [7], and vary the fraction $x_A = N_A/N$ of ABPs. Moreover, lengths are expressed in units of $2a$ and time in units of $1/D_r$.

3. Results

3.1. Phase behavior

A mixture of active and passive discs separates into a dense and a dilute phase at sufficiently large Pe, ϕ, and x_A [13], very similar to a pure ABP fluid [8]; in addition, active and passive particles tend to segregate inside the dense phase. This is illustrated in figure 1(a), where the segregation order parameter field $\Phi(\mathbf{r})$ of a large phase-separated system with curved interfaces between the dense and the dilute phase is shown. Φ is defined as $\Phi(\mathbf{r}) = (\phi_A - \phi_P)/(\phi_A + \phi_P)$ with coarse-grained packing density fields $\phi_A(\mathbf{r})$ and $\phi_P(\mathbf{r})$ of active and passive particles, respectively (see supplementary material for definition). The dilute phase consist mainly of passive particles ($\Phi \approx -1$) and the bulk of the dense phase is a homogenous active–passive mixture ($\Phi \approx 0$) with small patches of enriched active or passive particles. Within the interface region, we observe either an accumulation ($\Phi \approx 1$) or a depletion ($\Phi < 0$) of active particles.

3.2. Propagating interfaces in two-dimensional systems

The interfaces separating the high- and low-density phases of an active–passive mixture exhibit a remarkable dynamical behavior in a large region of the $\mathrm{Pe} - \phi - x_A$ parameter space. As indicated in figure 1(b), the interfaces propagate fast and coherently over large distances; see also supplementary movie `bulk_segregation_order.avi`. This is in contrast to the domain dynamics of an one-component ABP fluid in the steady state, which is limited to fluctuating interfaces resembling thermal capillary waves [12].

In order to quantify our observation, we analyse the density correlations by the dynamic structure factor $S(\mathbf{q}, \omega) = \int_{-\infty}^{\infty} F(\mathbf{q}, t)\exp(\mathrm{i}\omega t)\,\mathrm{d}t$, where $\mathbf{q}$ is the wavevector, ω is the angular frequency, and $F(\mathbf{q}, t) = \langle \rho_{\mathbf{q}}(t)\rho_{-\mathbf{q}}(0)\rangle/N$ is the collective intermediate scattering function (ISF) with the Fourier components $\rho_{\mathbf{q}}$ of the total particle density [27]. The angularly averaged $S(q, \omega)$, which is accessible by scattering experiments, is shown in figure 1(c). The structure factor exhibits peaks at the frequencies $\pm\omega_\rho$, with a width, characterized by $\Gamma(q)$, which increases with increasing q. This suggests a propagative excitation [27] related to the traveling interfaces indicated in figure 1(b). The full dispersion relations $\omega_\rho(q)$ and $\Gamma_\rho(q)$ follow from a fit of $F(q, t)$ to the functional form $F(q, 0)\exp(-\Gamma_\rho t)\cos(\omega_\rho t)$. Interestingly, the characteristic frequency exhibits a Brillouin-like dispersion relation $\omega_\rho = V_\rho q$ up to $q \approx 0.2$ with the velocity $V_\rho \approx 0.04V_0$, as displayed in figure 1(d), i.e., the interface moves with a constant velocity. The damping rate $\Gamma_\rho(q)$ obeys $\Gamma_\rho = D_\rho q^2$ up to $q \approx 0.2$, with the transport coefficient $D_\rho \approx 0.004D_0$, where $D_0 = D_t + V_0^2/(2D_r)$ is the diffusion constant of a free ABP. The damping rate Γ_ρ very likely originates from locally different propagation velocities and a decorrelation of the propagation directions, see figure 1(b). All excitations for $q > 0.25$ are very short lived, i.e, dense (or dilute) phase droplets with size smaller than about $50a$ dissolve quickly. In order to ensure that the observed Brillouin peaks do not originate from the persistent motion of the individual particles, we have also calculated the self-ISF [28]. The self-ISF shows only an exponential decay and contributes only to the collective-ISF at small length scales $q > 0.2$.

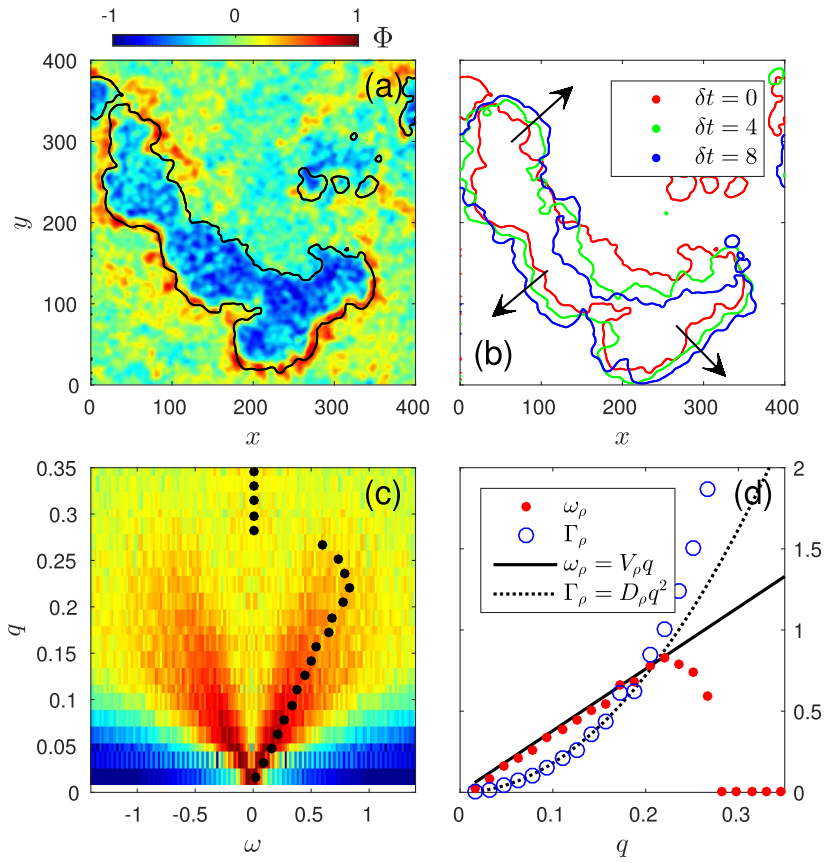

Figure 1. (a) Snapshot of the segregation order parameter field $\Phi(\mathbf{r})$ of a system of size $L_x = L_y = 400$ with $N = 160\,000$ particles ($\phi = 0.78$) in the steady state at $x_A = 0.5$. $\Phi = 1$ ($\Phi = -1$) corresponds to a pure active (passive) phase and $\Phi = 0$ to a uniform mixture. The black line indicates the interface position. (b) Time evolution of the interface position, see supplementary movie `bulk_segregation_order.avi`. (c) Dynamic structure factor $S(\omega, q)$ as a function of frequency ω and wavenumber q. The shape of $S(\omega, q)$ indicates a damped propagative mode. (d) Frequency ω_ρ (also indicated in (c) by black dots) and damping rate Γ_ρ as function of wavenumber. Lines indicate $\omega_\rho = V_\rho q$, with $V_\rho \approx 0.04 V_0$, and $\Gamma_\rho = D_\rho q^2$, with $D_\rho \approx 0.004 D_0$, where D_0 is the diffusion constant of a free ABP.

3.3. Propagating interfaces in quasi-one-dimensional systems

Further insight in the interface dynamics is obtained by studying an elongated box of lengths $L_x = 2L_y$ [12, 29] such that the interfaces favor to span the shorter box length, see figure 2. Given that the system phase-separates, such a configuration of a pair of interfaces—one enriched, the other depleted in active particles—forms spontaneously and remains stable over long time. Similar pairs of interfaces can also be identified in the two-dimensional system, as shown explicitly in figure S2 of the supplementary material.

In figures 3(a) and (b), we show the time evolution of the active-particle packing profile $\phi_A(x, t)$ averaged over the y-coordinate. Evidently, in case of a mixture both interfaces propagate steadily parallel to the right, in stark contrast to the diffusive motion of interfaces in a purely active fluid, see supplementary movies `positions_mixture.avi` and `positions_pure.avi`. The propagating interfaces are extremely stable within the typical simulation length of $T = 5 \times 10^3$, corresponding to 100 passes of the interface through the simulation box for $x_A = 0.5$; however, the propagation is occasionally interrupted by intermittent large-scale rearrangements of the interfaces. The propagation velocity V_{int} is nearly independent of the overall packing fraction ϕ and activity Pe as long as the system is phase separated (see figures S4–S6 of the supplementary material). However, V_{int} monotonously decreases with increasing x_A, with a maximum just above the active-particle fraction where phase separation sets in, see figure 3(c). The velocity V_ρ obtained from $S(q, \omega)$ is in agreement with V_{int} for $x_A \gtrsim 0.5$; however, V_ρ and V_{int} deviate from each other due to increasing nonlinearities in the dispersion relations $\omega_\rho(q)$ at low x_A near the transition, as shown in figure S3 of the supplementary material.

Figures 3(d)–(g) show profiles of various quantities calculated in a frame comoving with the interfaces, for both purely active fluids (dashed lines) and active–passive mixtures. In a pure active fluid, the two interfaces are equivalent and the polar vector $\langle e_x \rangle$, the average of the x-component of the propulsion direction, points preferentially into the dense phase, see figures 3(d) and (e). In a mixture, this symmetry is broken. Here, active particles preferentially accumulate at the advancing ('source') and deplete at the receding ('sink') interface, and

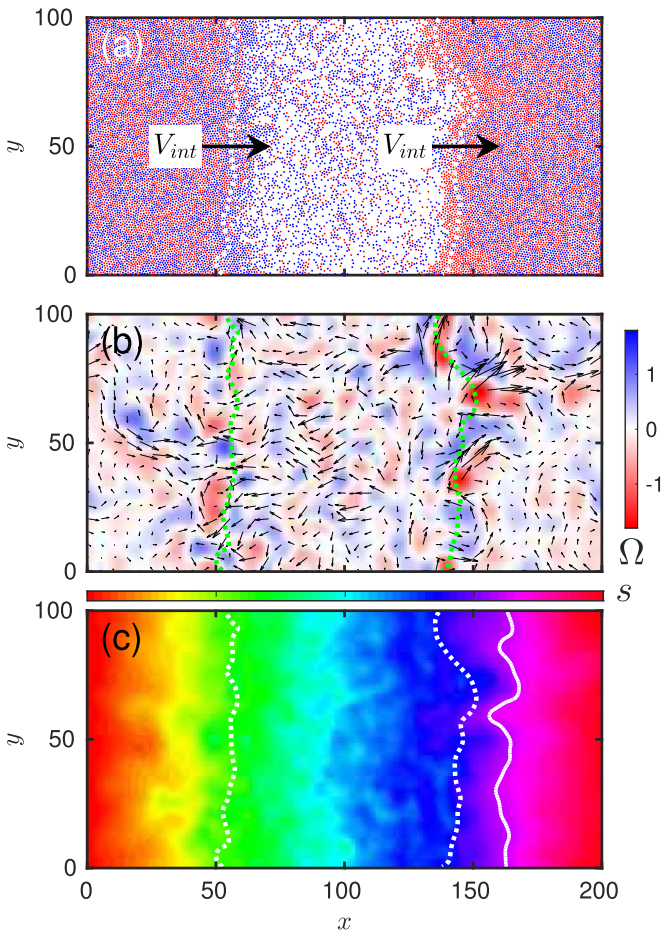

Figure 2. (a) Snapshot of a mixture of active (red) and passive (blue) Brownian discs at $x_A = 0.5$ in a box of size $L_x = 2L_y = 200$. The interfaces between the two phases (dashed lines (a)–(c)) travel by chance to the right. See supplementary movie `positions_mixture.avi`. (b) Vorticity $\Omega(\mathbf{r}) = \nabla \times \mathbf{J}(\mathbf{r})$, where $\mathbf{J}$ is the coarse-grained particle flux, see the supplementary material for definition and movie `vorticity_mixture.avi`. (c) Visualisation of the bulk flow. Particle positions are shown after the time lag $\delta t = 2$, where particles are colored according to their initial x position, as indicated by the color scale, see equation (2) for details. The solid line marks the isoline of $s(\mathbf{r}, \delta t)$ used for the stability analysis. See supplementary movie `mixing_mixture.avi`.

vice versa for passive particles. Similarly, the x-polarization $\langle e_x \rangle$ at both interfaces is different; it is larger at the advancing interface. Moreover, $\langle e_x \rangle$ takes negative values in the dilute phase, accompanied by a negative x-velocity of active particles, V_A, causing in turn a negative velocity of passive particles, V_P, due to collisions between passive and active particles, see figure 3(f). The mass transport from the dense into the dilute phase is characterized by the intensity of the particle flux vorticity $\mathcal{E}(x) = \int_0^{L_y} \Omega^2(\mathbf{r})\,\mathrm{d}y/L_y$ (see detailed discussion below), where $\Omega(\mathbf{r})$ is the curl of the particle flux $\mathbf{J}(\mathbf{r})$. $\mathcal{E}$ is most pronounced within the interface region and, in case of a mixture, $\mathcal{E}$ is larger at the side of larger polarization and active particle accumulation, see figures 3(g) and 2(b).

It is interesting to note that for stationary interface profiles in a co-moving reference frame, as shown in figures 3(d) and (f), there is a close relation between the packing density profiles $\phi_\alpha(x - V_{\mathrm{int}}t)$, the velocity profiles $V_\alpha(x - V_{\mathrm{int}}t)$, and the interfaces velocity V_{int}. In our elongated simulation box, $\phi_\alpha(x, t)$ obeys the one-dimensional continuity equation $\partial_t \phi_\alpha(x, t) + \partial_x J_\alpha(x, t) = 0$ with the particle flux $J_\alpha(x, t) = V_\alpha(x, t)\phi_\alpha(x, t)$, neglecting the diffusion term $D_t \partial_x \phi_\alpha(x, t)$ for high Péclet number Pe. We introduce a collective coordinate $\eta = x - V_{\mathrm{int}}t$, and obtain after integration

$$V_{\mathrm{int}}\phi_\alpha(\eta) + C_\alpha = J_\alpha(\eta) = V_\alpha(\eta)\phi_\alpha(\eta) \tag{1}$$

with integration constant C_α. Our simulation results are well consistent with the general result (1) for propagating interfaces, as shown in figure S8 of the supplementary material. Furthermore, when the flux is normalized such that it vanishes in the center of the dense phase, the flux of active particles within the dilute phase toward the *sink* interface is about twice as large as that for passive particles (for packing fraction $\phi = 0.67$). Nevertheless, there is no build-up of an active layer at the *sink* interface, as active particles are able to penetrate far into the dense phase, see figures 3(d) and (f) .

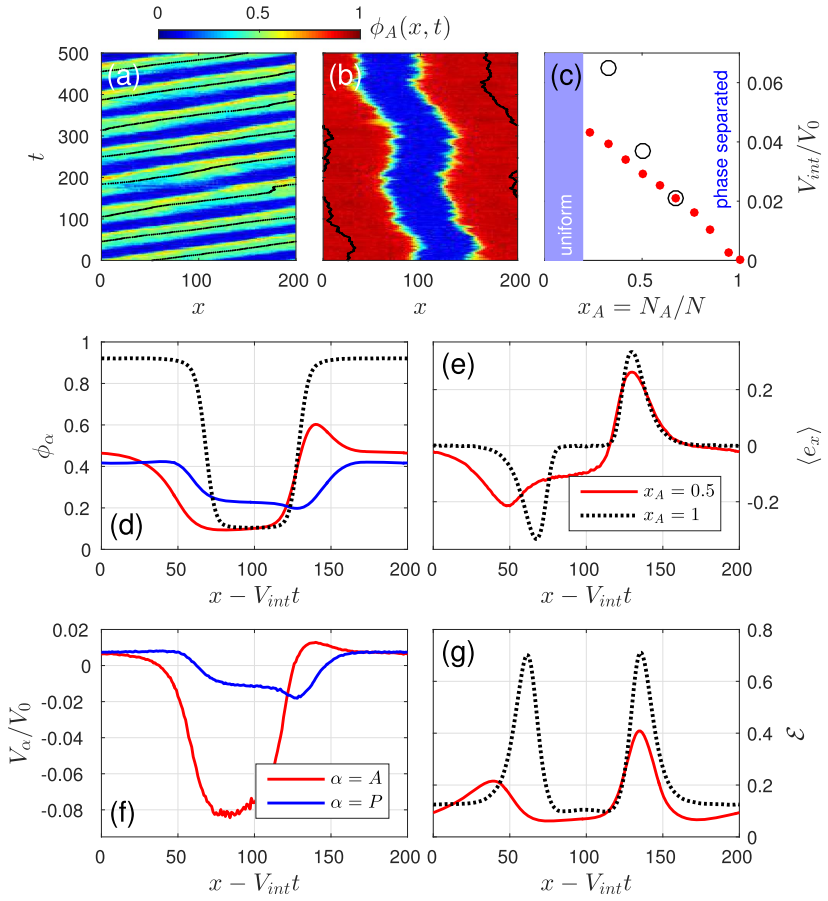

Figure 3. Space–time dependence of the active-particle packing density $\phi_A(x, t)$ for (a) the mixture with $x_A = 0.5$ and (b) a pure active fluid with $x_A = 1$. The black lines indicate the center-of-mass position of $\phi_A(x, t)$. (c) Velocities V_{int} (bullets) of the interface and V_ρ (circles) extracted from $S(q, \omega)$, see figure 1. Phase separation appears for $x_A \approx 0.2$. (d)–(g) Time averaged profiles measured in a comoving frame, i.e., relative to the propagating front, (d) of active- and passive-particle packing fractions $\phi_A(x - V_{int}t)$ and $\phi_P(x - V_{int}t)$, (e) of the active-particle x-polarization $\langle e_x \rangle(x - V_{int}t)$, (f) of active- and passive-particle velocities $V_A(x - V_{int}t)$ and $V_P(x - V_{int}t)$ along the interface propagation direction, and (g) of the intensity of the particle flux vorticity $\mathcal{E}(x - V_{int}t)$. We choose a representation, where the front propagates to the right. Solid lines correspond to $x_A = 0.5$ and dashed lines to $x_A = 1$.

4. Discussion

4.1. Interfaces in pure ABP fluids

Before discussing the possible mechanisms behind propagating interfaces, it is essential to consider interfaces in pure ABP fluids. Here the position of the interface is governed by the balance of incoming and outgoing fluxes; particles arrive at the interface from the dilute phase, remain oriented toward the dense phase for a while, and depart from the interface due to rotational diffusion [8]. This alone would generate a very rough and uncorrelated interface structure [25]. However, there is a smoothing mechanism; particles which bump into an undulated interface slide into regions of high convexity [9, 30, 31], and thereby level out the interface on small scales and produce a local polarization. In turn, this local polarization induces a mass flow inside the dense phase such that alternating vortices of opposite vorticity emerge within the interface region due to mass conservation, see figures 3(g) and 2(b) and supplementary movie `vorticity_pure.avi`. As a result, randomly oriented particles emerge from the bulk and cause an evaporation of the interface protrusions.

In order to quantify the vorticity-induced mass transport, we use the horizontal positions $x_i(t)$ of all particles at time t to construct the scalar field

$$s(\mathbf{r}, \delta t) = \frac{\sum_{i=1}^{N} x_i(t) f(\mathbf{r} - \mathbf{r}_i(t + \delta t))}{\sum_{i=1}^{N} f(\mathbf{r} - \mathbf{r}_i(t + \delta t))} \tag{2}$$

as function of time lag δt, where f is a Gaussian weight function, see the supplementary material. Thus, every particle i is marked at time t with its horizontal positions $x_i(t)$, i.e., every particle is flagged perennially by a label from the interval $[0, L_x]$ or by a color according to the colorbar in figure 2(c). At a later time $t + \delta t$, particles have moved to a new position $\mathbf{r}_i(t + \delta t)$; however, they still carry the label of their initial horizontal position $x_i(t)$. A completely mixed system appears monochrome. A similar passive scalar field was used to study fluid

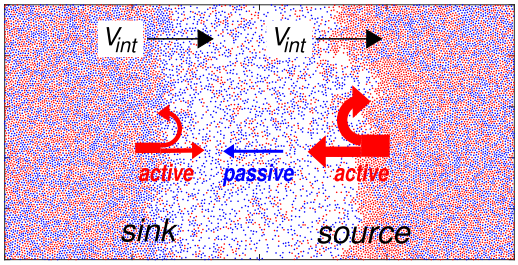

Figure 4. Illustration of the physical mechanisms underlying the formation of propagating interfaces in active–passive mixtures. At the more active (*source*) interface, randomly oriented active particle emerge from the bulk of the dense phase. Approximately half of them move toward the opposite interface, while the other half moves back. The flux of active particles form the *source* to the *sink* interface predominates the opposite flux. As a consequence, an imbalance of collisions of active with passive particle generates a flux of passive particles from the *source* to the *sink* interface.

mixing [32]. The temporal evolution of $s(\mathbf{r}, \delta t)$ then indicates the particle convection, see figure 2(c) and supplementary movie `mixing_pure.avi`. We choose a isoline of $s(\mathbf{r}, \delta t)$ inside the dense phase; this isoline is initially flat, but roughens as a function of time. This process is monitored by the Fourier modes of this isoline. The amplitudes of the undulation modes are found to grow with constant velocity $V_s(q)$ at short times. The growth velocities first increase with increasing q, reach a maximum at $q \approx 0.1$, and exhibit a fast decay for larger q, see figure 5(a). This confirms the visual impression in figures 2(b), (c) of a characteristic length scale of internal mass transport.

4.2. Interfaces in active–passive mixtures

The interface behavior changes drastically in mixtures: the profiles lack a symmetry and the interfaces propagate, see figure 3. We propose the following tentative explanation for this symmetry breaking , see figure 4. Consider an initially symmetric density profile with an active-particle corona at both interfaces. A local perturbation of the active-particle concentration or polarization within the corona leads to a larger outflux of active and passive particles from the more active (*source*) interface, due to the locally enhanced vorticity. Half of the randomly oriented active particles (figure 4), which emerge from the bulk of the dense phase, point away from the source interface and move toward the less active (*sink*) interface, while the other half moves back to the source interface and reinforces the active corona. Due to an imbalance of collisions of active with passive particles, a flux of passive particles is generated from the source to the sink interface (figure 4), and passive particles build up a corona at the sink interface. However, the overall packing density is lower at the sink interface, due to the excess of passive particles and a less pronounced active corona. Thus, incoming active particles penetrate this fluid-like layer of passive particles rather easily and do not build up an active corona, compare figure 3(d) and supplementary figure S8, such that the further discharge of active particles is inhibited. Finally, this feedback leads to a steady state, in which the actively generated mass flux sustains the interface propagation.

4.3. Nonequilibrium properties of the interface

We analyse the structure and dynamics of the interface by a Fourier transform of its fluctuations. We use a robust and unbiased approach to define the interface position by choosing an isoline of the overall packing density field, see dashed line in figure 2(a) and the supplementary material for further information. From the Fourier amplitudes h_q, we obtain the spectrum of the interfacial height fluctuations $\langle |h_q|^2 \rangle$ and the autocorrelation function $\langle h_q(t) h_{-q}(0) \rangle$, which we fit by $\langle |h_q|^2 \rangle \exp(-\Gamma_h t)$ to obtain the damping rate $\Gamma_h(q)$ as function of q. We observe a length-scale-dependent scaling $\langle |h_q|^2 \rangle \propto q^{-(1+2\alpha)}$ and $\Gamma_h \propto q^z$, where α and z are the roughness and the dynamic exponent, respectively [33]. We find $\alpha \approx 1/2$ and $z \approx 1.6$ on large scales, $q \lesssim 0.1$, and $\alpha \approx 1$ and $z \approx 2$ on intermediate scales, $0.1 \lesssim q \lesssim 0.4$, for static as well as propagating interfaces, see figures 5(b), (c). In comparison, for an overdamped fluid interface with thermally excited capillary waves in equilibrium, $\alpha = 1/2$ [29] and $z = 1$ [34] for $q < 0.6$. However, physically more related is the Edward–Wilkinson model [25, 26] for non-equilibrium interface growth with $\alpha = 1/2$ and $z = 2$, where random particle deposition leads to interface roughening, while lateral motion (e.g., due to gravity) yields interface smoothing. If additionally local growth perpendicular to the interface is present, as in the Kardar–Parisi–Zhang model, the dynamic exponent $z = 3/2$ is expected [25, 26], very close to the exponents characterizing the interface behavior of our active particle fluids.

The spectrum $\langle |h_q|^2 \rangle$ of interface undulations in figure 5(b) demonstrates that propagating interfaces fluctuate more strongly than non-propagating interfaces. In order to emphasize this difference, we present in figure 6(a) the interfacial width $w^2 \approx \sum_q \langle |h_q|^2 \rangle$ as a function of system size L_y. For interfaces in two-dimensional equilibrium systems, $w^2 \propto L_y$ [35]. As a consequence of $\langle |h_q|^2 \rangle \propto q^{-2}$ we observe the same linear scaling of w^2

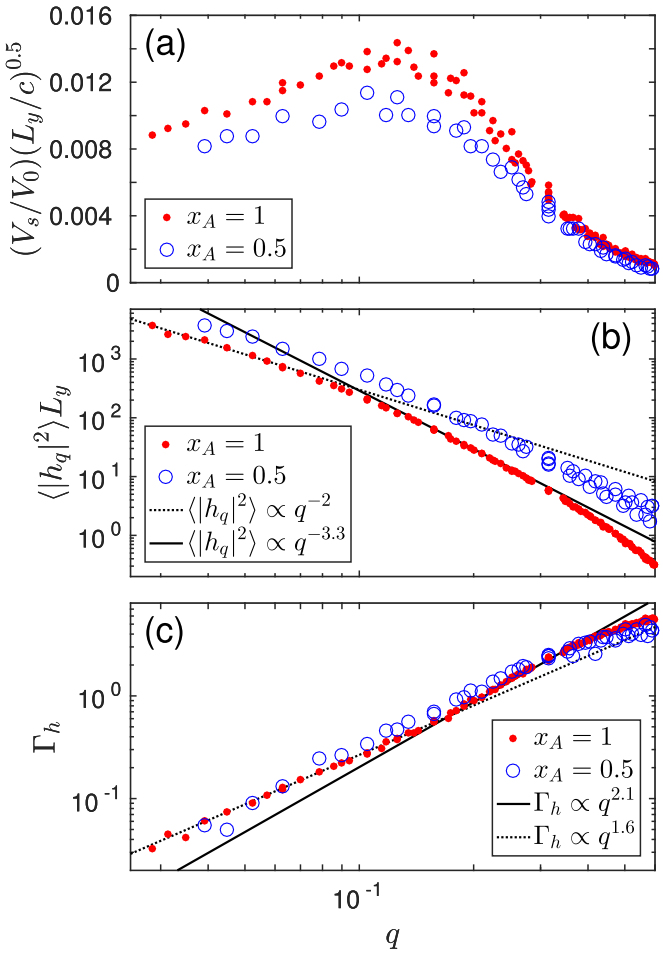

Figure 5. (a) Growth velocities $V_s(q)$ of the Fourier modes of an isoline of the passive scalar field $s(\mathbf{r}, \delta t)$ inside the dense phase, see equation (2) and figure 2(c). (b) Spectrum of the interfacial height fluctuations $\langle |h_q|^2 \rangle$ as a function of the wave number q; results for different L_y at fixed L_y/L_x are shown. (c) Decay rate $\Gamma_h(q)$ of the interfacial height autocorrelation function $\langle h_q(t) h_{-q}(0) \rangle$. Different scaling regimes are indicated by lines.

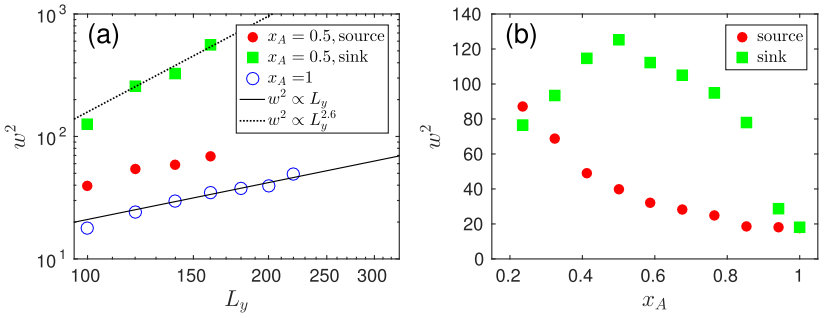

Figure 6. (a) Interfacial width w^2 as a function of system size L_y for a mixture ($x_A = 0.5$, filled symbols) and a pure active fluid ($x_A = 1$, open symbols). (b) w^2 versus x_A.

in active systems, both for non-propagating interfaces ($x_A = 1$) [12] and for source interfaces in active–passive mixtures ($x_A = 0.5$). However, sink interfaces in mixtures ($x_A = 0.5$) are much rougher than source interfaces as well as interfaces in purely active systems—with their width growing superlinearly as $w^2 \propto L_y^{2.6}$. Note that the steady propagation of parallel interfaces becomes unstable for $L_y > 160$, compare figure S4(c) in the supplementary material, which of course implies that the scaling relations break down at this system size. The roughness of both source and sink interfaces increases with decreasing fraction x_A of active particles from $x_A = 1$ to $x_A \simeq 0.5$, see figure 6(b); however, for sink interfaces, w^2 starts to decrease again for $x_A \lesssim 0.5$. Note

that interfaces disappear for $x_A < 0.2$ due to vanishing phase separation; the interface width of the two types of interfaces becomes essentially identical in this limit.

5. Summary and conclusions

Active-particle systems display a variety of novel and unexpected features—both static and dynamic. This particularly applies to mixtures of active and passive particles. In the present study, we focused on the collective dynamical behavior of such mixtures in the phase separated state. We have shown that the large-scale interface structure in mixtures is similar to that at equilibrium, with an undulation spectrum proportional to q^{-2} for small wave vectors q. However, the dynamics, like interface relaxation and propagation, exhibits strong nonequilibrium characteristics. In particular, we find a spontaneous symmetry breaking between source and sink interfaces. Here, the source interface is enriched in active Brownian particles, propagates toward the dense phase, and generates a steady flux of active and passive particles into the dilute phase, while the sink interface is depleted of active particles, propagates toward the dilute phase, and receives a steady influx of active and passive particles. The propagation velocity is a function of the active particle fraction x_A, which decreases with increasing x_A, and vanishes in a purely active system (where the interface dynamics becomes diffusive).

Besides the interface propagation there are further dynamical features like the surprising oscillations of the center-of-mass position of the interface as well as the interface width (see figure S9 of supplementary material), which does not have a simple explanation. This calls for further theoretical investigations, for example, via an extension of the mean-field theory for a suspension of active particles [36] to active–passive mixtures.

Our results should be relevant and helpful for the interpretation of experiments of mixtures of passive and active colloids [3–6, 18], polar and apolar vibrated disks [37] or even specially programmed robots [38, 39]. Thereby, the interface propagation can be identified via $S(\mathbf{q}, \omega)$ in scattering experiments or by direct observation. In order to study the interface propagation in experiments, we recommend a racetrack setup [40], which mimics a quasi-one-dimensional system with periodic boundary conditions. Simulations show that for narrow channels the propagation forms spontaneously and remains stable over long time, see supplementary movie `channel_mixture.avi`.

Acknowledgments

We thank A Varghese (FZ Jülich), J Horbach (HHU Düsseldorf) and R Wittkowski (WWU Münster) for helpful discussions. Support by the DFG priority program SPP1726 on 'Microswimmers' is gratefully acknowledged.

References

[1] Elgeti J, Winkler R G and Gompper G 2015 *Rep. Prog. Phys.* **78** 056601
[2] Marchetti M C, Fily Y, Henkes S, Patch A and Yllanes D 2016 *Curr. Opin.Colloid Interface Sci* **21** 34–43
[3] Theurkauff I, Cottin-Bizonne C, Palacci J, Ybert C and Bocquet L 2012 *Phys. Rev. Lett.* **108** 268303
[4] Palacci J, Sacanna S, Steinberg A P, Pine D J and Chaikin P M 2013 *Science* **339** 936–40
[5] Buttinoni I, Bialké J, Kümmel F, Löwen H, Bechinger C and Speck T 2013 *Phys. Rev. Lett.* **110** 238301
[6] Ginot F, Theurkauff I, Levis D, Ybert C, Bocquet L, Berthier L and Cottin-Bizonne C 2015 *Phys. Rev.* X **5** 011004
[7] Fily Y, Henkes S and Marchetti M C 2014 *Soft Matter* **10** 2132–40
[8] Redner G S, Hagan M F and Baskaran A 2013 *Phys. Rev. Lett.* **110** 055701
[9] Wysocki A, Winkler R G and Gompper G 2014 *Europhys. Lett.* **105** 48004
[10] Cates M E and Tailleur J 2015 *Annu. Rev. Condens. Matter Phys.* **6** 219–44
[11] Stenhammar J, Marenduzzo D, Allen R J and Cates M E 2014 *Soft Matter* **10** 1489–99
[12] Bialké J, Siebert J T, Löwen H and Speck T 2015 *Phys. Rev. Lett.* **115** 098301
[13] Stenhammar J, Wittkowski R, Marenduzzo D and Cates M E 2015 *Phys. Rev. Lett.* **114** 018301
[14] Angelani L, Maggi C, Bernardini M L, Rizzo A and Di Leonardo R 2011 *Phys. Rev. Lett.* **107** 138302
[15] Peng Y, Lai L, Tai Y S, Zhang K, Xu X and Cheng X 2016 *Phys. Rev. Lett.* **116** 068303
[16] Das A, Polley A and Rao M 2016 *Phys. Rev. Lett.* **116** 068306
[17] Ni R, Cohen Stuart M A, Dijkstra M and Bolhuis P G 2014 *Soft Matter* **10** 6609–13
[18] Kümmel F, Shabestari P, Lozano C, Volpe G and Bechinger C 2015 *Soft Matter* **11** 6187–91
[19] Takatori S C and Brady J F 2015 *Soft Matter* **11** 7920–31
[20] Grosberg A Y and Joanny J F 2015 *Phys. Rev.* E **92** 032118
[21] Weber S N, Weber C A and Frey E 2016 *Phys. Rev. Lett.* **116** 058301
[22] Tanaka H, Lee A A and Brenner M P 2016 arXiv:1611.02234
[23] Yang X, Manning M L and Marchetti M C 2014 *Soft Matter* **10** 6477–84
[24] van der Meer B, Prymidis V, Dijkstra M and Filion L 2016 arXiv:1609.03867
[25] Barabási A and Stanley H 1995 *Fractal Concepts in Surface Growth* (Cambridge: Cambridge University Press)
[26] Krug J 1997 *Adv. Phys.* **46** 139–282
[27] Hansen J and McDonald I 1990 *Theory of Simple Liquids* (Amsterdam: Elsevier)

[28] Paoluzzi M, Leonardo R D and Angelani L 2013 *J. Phys.: Condens. Matter* **25** 415102
[29] Vink R L C, Horbach J and Binder K 2005 *J. Chem. Phys.* **122** 134905
[30] Fily Y, Baskaran A and Hagan M F 2014 *Soft Matter* **10** 5609–17
[31] Nikola N, Solon A P, Kafri Y, Kardar M, Tailleur J and Voituriez R 2016 *Phys. Rev. Lett.* **117** 098001
[32] Saintillan D and Shelley M J 2008 *Phys. Fluids* **20** 123304
[33] Siegert M 1996 *Phys. Rev.* E **53** 3209–14
[34] Gross M and Varnik F 2013 *Phys. Rev.* E **87** 022407
[35] Flekkøy E G and Rothman D H 1995 *Phys. Rev. Lett.* **75** 260–3
[36] Farrell F D C, Marchetti M C, Marenduzzo D and Tailleur J 2012 *Phys. Rev. Lett.* **108** 248101
[37] Deseigne J, Dauchot O and Chaté H 2010 *Phys. Rev. Lett.* **105** 098001
[38] Rubenstein M, Cornejo A and Nagpal R 2014 *Science* **345** 795–9
[39] Mijalkov M, McDaniel A, Wehr J and Volpe G 2016 *Phys. Rev.* X **6** 011008
[40] Bricard A, Caussin J B, Desreumaux N, Dauchot O and Bartolo D 2013 *Nature* **503** 95–8